analytical chemistry

Article

pubs.acs.org/ac

Following a Folding Transition with Capillary Electrophoresis and Ion Mobility Spectrometry

John D. Barr,[†] Liuqing Shi,[‡,∥] David H. Russell,[§] David E. Clemmer,[‡] and Alison E. Holliday*[,†]

[†]Department of Chemistry, Moravian College, Bethlehem, Pennsylvania 18018, United States

[‡]Department of Chemistry, Indiana University, Bloomington, Indiana 47405, United States

[§]Department of Chemistry, Texas A&M University, College Station, Texas 77843, United States

Supporting Information

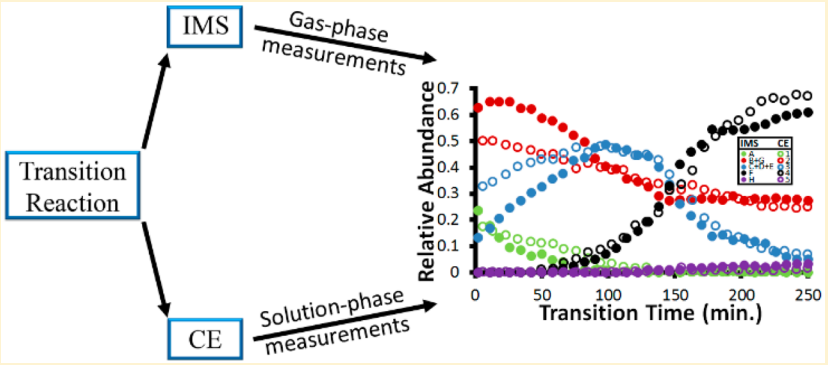

ABSTRACT: Ion mobility spectrometry (IMS) is increasingly used to describe solution-phase phenomena and has recently been used to establish the presence of multiple intermediates during the folding of a model polypeptide, polyproline. These observations, however, are made on gas-phase structures. Capillary electrophoresis (CE) is a complementary solution-phase technique, also based on the separation of charged species as a function of size and charge. Here, both ion mobility and capillary electrophoresis are used to follow the folding transition of a 13-mer polyproline peptide from the all-*cis* polyproline I (PPI) conformation to the all-*trans* polyproline II (PPII) conformation upon immersion in aqueous solvent. Synchronous folding processes are observed using both techniques. Eight conformers are observed using ion mobility. Although only five peaks are observed using capillary electrophoresis, these peaks can be modeled as sums of the observed IMS conformers; this is strong evidence that ion mobility is sampling solution-phase structures. CE measurements provide the first direct evidence that multiple folding intermediates are present in solution.

Mass spectrometry (MS) is commonly paired with ion mobility spectrometry (IMS) to allow resolution of complex protein and peptide structures.[1−4] Electrospray ionization (ESI) is used as a "soft" method capable of transferring solution-phase peptide populations into the gas phase,[5−8] and multiple groups have shown that solution-phase structures of peptides can be separated using IMS based on differences in their resulting gas-phase collision cross sections.[9−12] These collision cross sections are correlated with an ion's overall shape, and experimentally determined values can be compared to cross sections calculated for trial geometries generated by theoretical techniques like molecular dynamics.[13,14] Although differences between native solvated structures and gas-phase structures may arise through desolvation, there is evidence that subpopulations present in the solution can be investigated, as they are "freeze dried" and constrained along the energy surface as they are transferred to the gas phase.[15] An example of this approach is our recent study using IMS-MS to observe eight structurally distinct conformers during the folding transition of a model polypeptide, a 13-residue polyproline (Pro13).[16]

To this point, connections between the measured gas-phase structure and the original solution-phase structure have been established through computational approaches[13,14] and through experimental observation of structural shifts as water is removed.[15,17] Thus, studies of gas-phase conformations have led to a better understanding of protein and peptide behavior in solution,[18−21] but definitive evidence that IMS-MS provides direct information about solution-phase processes is lacking. We propose that capillary electrophoresis (CE) can strengthen the link, as CE is the solution-phase analogue of IMS. Similar to IMS, ions are separated based on their size and charge, but CE separates species based on differences in their solvated hydrodynamic radius instead of the gas-phase collision cross sections of IMS. CE can resolve cis/trans isomers of a molecule containing a single proline peptide bond[22] and can be used to differentiate between folded and fully unfolded states of

Received: June 23, 2016
Accepted: October 24, 2016
Published: November 4, 2016

DOI: 10.1021/acs.analchem.6b02424
Anal. Chem. 2016, 88, 10933−10939

proteins.[23] CE has been used to observe and monitor conformational changes resulting from differential exposure to denaturing conditions, including the formation of multiple non-native states.[24−30] Kinetic CE methods have also been used to monitor the slow ligand-induced interconversion of conformations of a protein,[31] and intermediates have been observed upon formation of a multimeric protein from monomer subunits.[32] CE has provided evidence of a single time-based folding intermediate for a protein,[28] but multiple intermediate folding conformations have not been previously observed.

In this work, both IMS and CE are used to investigate the conformational transitions that occur during folding of Pro13. Unlike other amino acids, proline shows a propensity to also take the cis conformation when forming peptide bonds.[33] As a result, polyproline chains have two major conformational forms:[34] the polyproline I (PPI) helix, a right-handed helix with all peptide bonds in the cis conformation which is favored in hydrophobic environments,[35] and the polyproline II (PPII) helix, a left-handed helix with all peptide in the trans conformation which is favored in aqueous environments.[36,37] Switching solvent environments initiates folding of the peptide from one helical form to the other. Since the energy barriers for cis-trans isomerization of proline are high,[38] the PPI → PPII transition is slow enough to enable monitoring. As a result, the first experimental observation of multiple intermediates in peptide folding was on this system, using ion mobility spectrometry.[16] Confirmation that these multiple intermediates are present in solution, rather than being gas-phase observational artifacts, is thus particularly important.

Using CE, five different peaks can be observed during the transition from solid PPI to aqueous PPII, although they are not fully resolved. The profiles of conformer abundance as a function of time are remarkably similar for the direct solution-phase measurements of CE and the measurements of desolvated structures by IMS-MS. A direct comparison between the IMS measurements and CE results confirms the existence of polyproline folding intermediates in solution.

EXPERIMENTAL SECTION

Sample Preparation. Pro13 was synthesized following an established Boc solid-phase peptide protocol, as described previously.[39] Additional Pro13 was obtained from GenScript (Piscataway, NJ) for CE experiments. Pro13 samples were dissolved in excess 1-propanol and incubated at room temperature for 72 h to generate the PPI conformer.[16] The solution was then dried under a stream of air (CE experiments) or by vacuum centrifugation (IMS experiments) to obtain a solid sample. The solid starting material was necessary to obtain adequate solution-phase concentrations for detection in the CE experiments. The transition process was initiated by adding a 15 °C solution of 10/88/2 1-propanol/H_2O/HOAc (v/v/v) to the solid Pro13 to obtain a final concentration of 800 μM (CE experiments) or 16 μM (IMS experiments). The sample was vortexed to ensure complete dissolution at the start of the transition. The solvent composition was chosen to facilitate electrospray ionization for IMS experiments as well as to enable comparison to prior IMS experiments on polyproline folding in solution.[16] The resulting solution was maintained at 15 °C throughout the transition. Parallel CE and IMS-MS experiments were carried out separately; each was run in triplicate. One additional CE experiment was run at a concentration of 400 μM.

Ion-Mobility Spectrometry. The experiment was carried out on a home-built IMS-MS instrument, as has been previously described.[40] At defined time intervals during the transition, aliquots were pipetted into the sample tray of a TriVersa NanoMate autosampler (Advion, Ithaca, NY) held at 4 °C. Samples were then immediately electrosprayed and then trapped and accumulated in a Smith-geometry hourglass ion funnel.[41] These accumulated ion packets were then periodically pulsed (150 μs) into an ∼1.8 m drift tube containing ∼3.0 Torr of helium buffer gas held at 300 K. Separation occurred under an electric field of ∼10 V cm^{-1}, and ions exiting the drift region were extracted into an orthogonal reflectron time-of-flight mass spectrometer for detection. Flight times in the mass analysis region are comparably shorter than drift times, making it possible to collect the data in a nested fashion, as has been previously described.[42]

Collisional cross sections (CCS, Ω) were determined from experimental drift times, t_D, using eq 1:[43]

$$\Omega = \frac{(18\pi)^{1/2}}{16}\frac{ze}{(k_bT)^{1/2}}\left[\frac{1}{m_1}+\frac{1}{m_b}\right]^{1/2}\frac{t_DE}{L}\frac{760}{P}\frac{T}{273.2}\frac{1}{N} \quad (1)$$

where k_b is Boltzmann's constant, T is the temperature of the buffer gas, ze is the charge on the ion, m_I is the mass of the ion, m_B is the mass of the buffer gas, E is the applied electric field over the drift tube of length L, P is the buffer gas pressure, and N is the neutral number density of the buffer gas at STP. The relative abundance of each observed conformer at each transition time was calculated using the Peak Analyzer tool in OriginPro 9.0.0 (OriginLab Corporation, Northampton, MA).

Capillary Electrophoresis. A commercial Beckman Coulter PA800 capillary electrophoresis system with UV−vis detection was used for separations. The fused silica capillary (i.d. 50 μm, Polymicro Technologies, Phoenix, AZ) had 31.2 cm total length, with a distance to the detector of 21.0 cm. The capillary and sampling tray were maintained at a constant temperature of 15 °C throughout the experiment. The background electrolyte (BGE) was the same 10/88/2 1-propanol/H_2O/HOAc (v/v/v) solution used to initiate the transition. This choice was made to ensure that additional conformational or charge-state changes would not occur due to interactions of polyproline with the BGE. The capillary was conditioned beforehand by rinsing with 0.1 M NaOH for 10 min, followed by H_2O for 10 min, and last BGE for 20 min. A solution containing dibenzylamine and 3-ethylphenol in BGE was coinjected with the Pro13 solution to provide a positive and neutral marker for the separation; this was used to measure electroosmotic flow (EOF) during the separation and to ensure reproducibility of peak migration after correcting for EOF variation. The dibenzylamine/3-ethylphenol solution and Pro13 solution were sequentially hydrodynamically injected using 0.5 psi for 5 s. After injection, a 5 min separation was run with an applied voltage of +30 kV; the electropherogram was recorded with detection at 209 nm. This short separation time was necessary to ensure that separation occurred on a faster time scale than conformation changes during the transition. Between separations, the capillary was rinsed with BGE for 1 min. Repeat analyses of the sample solution occurred until no further changes were observed in the resulting electropherograms.

Analysis of CE Data. Overlapping peaks can be observed in experimental electropherograms. Using the Peak Analyzer tool in OriginPro 2015 (OriginLab Corporation, Northampton, MA), the Pro13 distribution within each electropherogram was deconvoluted to obtain information about underlying peaks. Iterative deconvolution fits were run until the reduced chi-

DOI: 10.1021/acs.analchem.6b02424
Anal. Chem. 2016, 88, 10933−10939

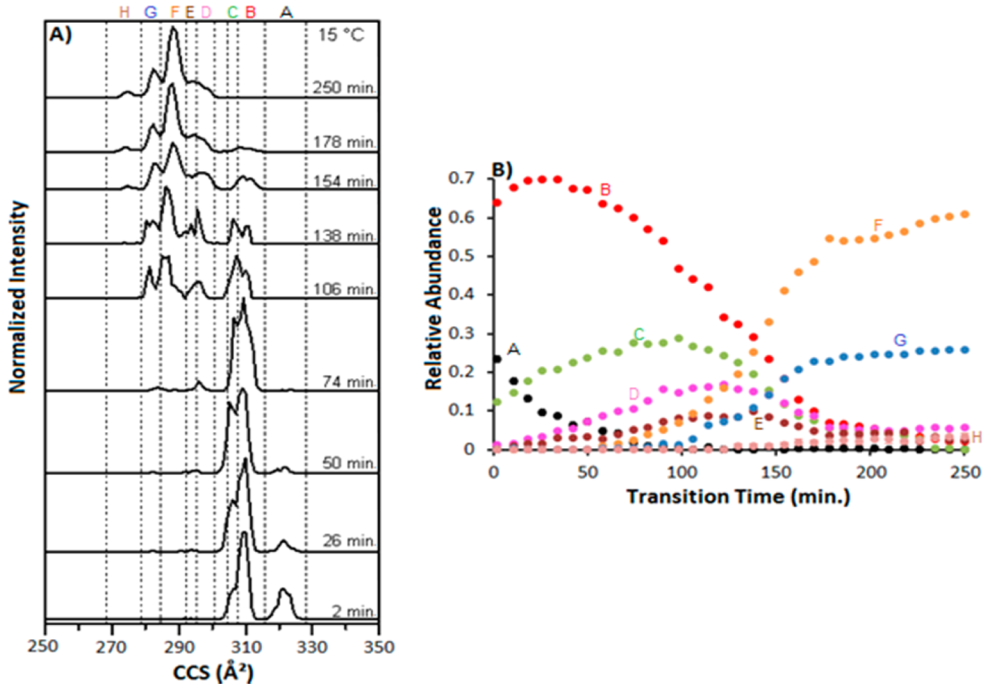

Figure 1. (A) CCS distributions for desolvated gas-phase Pro13 obtained at different transition times from a PPI(s) to PPII(aq) transition in 10/88/2 1-propanol/H_2O/HOAc (v/v/v) at 15 °C, as observed using IMS. (B) Relative abundance of each conformer type defined in the CCS distributions as a function of transition time. The relative abundance is calculated for a given species by dividing the area under the curve of that species by the total area for all Pro13 species at that time point. Various colors are used to represent different conformers: A is black, B is red, C is green, D is magenta, E is maroon, F is orange, G is blue, and H is rose.

squared value between the sum of the underlying peaks and the experimental electropherogram was minimized, ensuring the best possible fit for a set of data. A typical fit would be considered to have converged when a change in chi-squared, or tolerance, between successive iterations was less than a value of 10^{-12}. Resulting fits had chi-squared values between 6×10^{-9} and 2×10^{-8}. Optimized underlying peak functions were then plotted using Maple 17 (Maplesoft, Waterloo, ON, Canada), as the graphical output from Peak Analyzer plotted insufficient points.

In CE, electromigration dispersion is known to cause peak asymmetry, leading to triangular peak shapes that broaden and become more distorted with increasing concentration.[44−47] Diffusion is a second source of peak broadening, generating a Gaussian distribution for analyte peaks. Both types of broadening can be experimentally observed in the distorted shapes of the positive marker (dibenzylamine) peak and final equilibrium Pro13 distribution. The Haarhoff-Van der Linde (HVL) function is used to fit and describe CE peaks with both types of broadening present.[48−50] The full HVL function is described in the Supporting Information. The function has four adjustable parameters: the peak center (x_c), area (A), width (w), and distortion (d). The parameters w, A, and d are concentration-dependent parameters[48−50] and were thus left unfixed, so that the fitting algorithm could freely modify them between successive electropherogram fits. The x_c parameter is independent of analyte concentration, and it represents the "true" migration time of an analyte since it will be the observed peak center in cases where no asymmetric triangular distortion is observed ($d \approx 0$).[48−50]

Preliminary testing was done to establish the number of peaks in the deconvolution. Local minima in the second derivative of the Pro13 distribution were used to establish the presence of four underlying features (peaks 1−4) in a majority of electropherograms. A fifth peak (peak 5) was observed at long transition times. However, this set of peaks was inadequate to model the distribution (Figure S1), and satisfactory reduced chi-squared values were not obtained. The distribution shows distinct tailing at all transition times, and thus a sixth peak (the tail) was added to complete the model. Fitting with a fewer number of peaks failed to lead to fits that could adequately describe experimental electropherograms. Fitting with a larger number of peaks either led to additional peaks being minimized so that only six peaks would contribute to the fit or the fit would fail to lead to a satisfactory chi-squared value (Figure S1).

Shifts in the electroosmotic flow can be observed between successive separations, as indicated by the change in position of the neutral peak; this causes slight variance in migration time for other species (Figure S2). Such shifts in electroosmotic flow are not uncommon.[51] However, by fixing the peak center for each peak about a ±5 s interval, the same five Pro13 peaks successfully fit the Pro13 distributions throughout the transition. As described below, calculation of electrophoretic mobilities of all peaks confirmed the viability of this approach.

The resulting peaks from these fits were integrated to obtain the area under the curve. An adjusted area for a given species was then calculated by dividing the integrated area by the peak's respective migration time, x_c. This transformation helps correct for the fact that, in CE, each species will move through the detector region with different velocity.[49,50] The relative abundance of each contributing peak was calculated by dividing the adjusted area of the peak by the total area of the Pro13 distribution. Abundance profiles for each peak were then generated by plotting the relative abundance of a peak against transition time.

Determination of Electrophoretic Mobility. As noted above, changes in EOF caused slight changes in peak position on

DOI: 10.1021/acs.analchem.6b02424
Anal. Chem. 2016, 88, 10933−10939

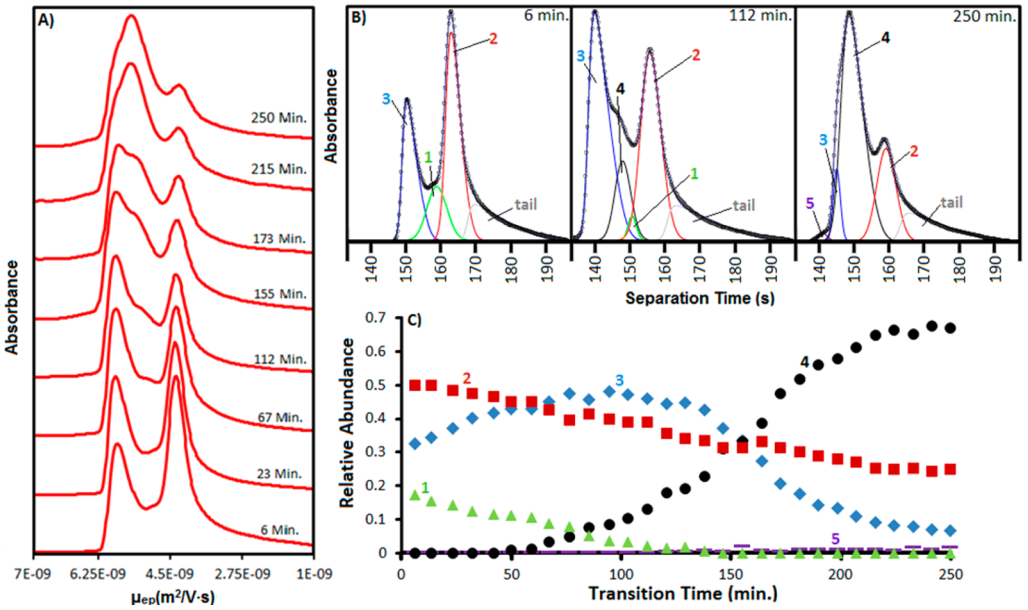

Figure 2. (A) Experimental electropherograms converted to an electrophoretic mobility scale at different transition times for a PPI(s) to PPII(aq) transition in 10/88/2 1-propanol/H_2O/HOAc (v/v/v) at 15 °C, as observed using CE. (B) Fits of experimental electropherograms at various transition times, where each colored peak represents an underlying contributing peak from peak deconvolution: 1 is green, 2 is red, 3 is blue, 4 is black, and 5 is purple. Experimental data are represented as black circles, and the navy line is the sum of the five peaks and the tail from peak deconvolution. (C) Relative abundance of underlying peaks as a function of transition time, as found with CE; each species in the abundance profile corresponds to the peak defined by the same number and color in the experimental fits. The relative abundance is calculated for a given species by dividing the adjusted area under the curve of that species by the total area for all Pro13 species at that time point.

the time axis, and so electrophoretic mobilities were calculated for each observed peak to ensure reproducible identification. Experimental apparent mobilities, μ_{app}, were calculated by dividing the distance to the detector by the species' observed migration time, t_{app}, and the electric field (E) generated by the applied voltage over the length of the capillary. μ_{app} was then related to the species' electrophoretic mobility, μ_{ep}, using eq 2:[52]

$$\mu_{ep} = \mu_{app} - \mu_{eo} \quad (2)$$

where μ_{eo} is the electroosmotic mobility, a bulk property which was calculated by dividing the distance to the detector by the migration time of the neutral species (t_n), and E. Each experimental electropherogram was converted from an absorbance vs time plot to an absorbance vs μ_{ep} plot.[51] The new x-axis accounts for differences in EOF between separations to ensure the reproducibility of the migration for the observed Pro13 species.

Hydrodynamic Radius. A species' hydrodynamic radius (R_h) and effective charge (q) are related to μ_{ep} through eq 3:[53]

$$\mu_{ep} = \frac{q}{6\pi\eta R_h} \quad (3)$$

where η is the dynamic viscosity of the solution in the capillary. Variables η and E were held constant throughout the transition. The dynamic viscosity, η, for the 10/88/2 1-propanol/H_2O/HOAc solution at 15 °C was calculated by multiplying the measured kinematic viscosity by the measured density of the solution at 15 °C. The kinematic viscosity was determined by measuring the efflux time from a Cannon-Fenske Viscometer submerged in a 15 °C bath; replicate analyses were done using standard water as well as the 10/88/2 1-propanol/H_2O/HOAc (v/v/v) solution.[54] Although the applied voltage will affect the viscosity, the effect should be equivalent across all experiments at a given applied voltage.

The hydrodynamic radius is the radius of a hard sphere with equivalent frictional properties. Using eq 4,[55,56] a theoretical hydrodynamic radius can also be calculated for structures with a rod-like or cylindrical shape:

$$R_h = L\left(\frac{3}{16p^2}\right)^{1/3}(1.009 + 0.01395(\ln p) + 0.078880(\ln p)^2 + 0.006040(\ln p)^3) \quad (4)$$

where L is the length of the cylinder, and p is the ratio of the cylinder's length to its diameter.

RESULTS AND DISCUSSION

Using IMS, eight different conformers (A-H) of $[Pro13 + 2H]^{2+}$ were observed during the transition of PPI(s) to PPII(aq) (Figure 1A). Only the 2+ charge state was observed using IMS-MS. On the basis of their collision cross sections, these conformers were assigned as having the same gas-phase structures previously observed during the transition of PPI(propanol) → PPII(aq).[16] Conformer A is assigned as PPI, and conformer F is assigned as PPII.[16]

Integration of each conformer at each transition time point (Figure 1B) yields profiles that are also consistent with the mechanism proposed for the PPI(propanol) → PPII(aq) transition.[16] Starting with conformer A (PPI), a sequential loss of conformers with larger gas-phase collision cross sections is observed; this culminates in the establishment of an equilibrium population dominated by conformers F (PPII) and G. However, starting the transition with PPI(s) leads to some differences in conformer relative abundance at short transition times, as compared to transitions initiated from propanol solutions,[16] notably a reduced initial abundance of conformer A (PPI) and a corresponding increase in initial abundance of transition

DOI: 10.1021/acs.analchem.6b02424
Anal. Chem. 2016, 88, 10933−10939

intermediates B and C. The process of drying propanol solutions to obtain PPI(s) has an effect on which conformations are present; it appears that the transition toward PPII is already underway when the experiment is initiated by dissolution of the solid in 10/88/2 1-propanol/H_2O/HOAc (v/v/v). The solid starting material was necessary to obtain adequate solution-phase concentrations for detection in the CE experiments.

Using peak deconvolution of the CE data, five components (1−5) were partially resolved in the Pro13 distribution during the transition from PPI(s) to PPII(aq) (Figure 2A,B). This is the first direct observation of multiple intermediates in protein folding in solution. As shown in Figure 2C, the abundance of these components changed as a function of time. The abundance profiles are complex and will be explored in detail below. A tailing component to the Pro13 distribution was also present and consistent throughout the experiment (Figure S3) and thus was not included in further data analysis.

Figure 3 is a comparison of the abundance profiles generated by monitoring the transition from PPI(s) to PPII(aq) using IMS and CE. As fewer resolved components are observed in CE than in IMS, we have added the relative abundances of conformers observed using IMS (as shown in Figure 1) to model the distribution seen in CE. Here, we present the combinations that provide the closest fit between the two data sets; alternative combinations with inferior fits are found in the Supporting Information (Figure S4).

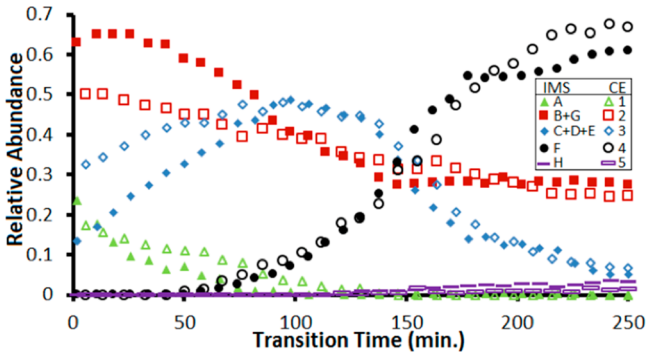

Figure 3. Comparison of relative abundance of conformers as a function of transition time for the transition from PPI(s) to PPII(aq) in 10/88/2 1-propanol/H_2O/HOAc (v/v/v) at 15 °C monitored using IMS (filled symbols) and CE (hollow symbols). Note that the relative abundance of IMS conformers in Figure 1 are combined in this figure. Each species from CE is colored to match the species or combination from IMS that behaves notably similar.

Peak 1 from CE, which has an average electrophoretic mobility of $(4.79 \pm 0.05) \times 10^{-9}$ m^2/V s, has a relative abundance of about 0.2 at the start of the transition. From here, peak 1 decreases over time and becomes nearly unobservable after 110 min. This closely corresponds to the loss of peak A, assigned to the PPI helix,[16] in the IMS data. At the start of the transition, peak A has a relative abundance of about 0.25 and it becomes vanishingly small after 90 min.

Peak 2 from the CE data, which has an average electrophoretic mobility of $(4.18 \pm 0.06) \times 10^{-9}$ m^2/V s, starts at a relative abundance of about 0.5 and decreases until it reaches a steady abundance of about 0.3 between 150 and 250 min. This trend in abundance favorably compares to a combination of conformers B and G from the IMS data; the sum of relative abundances of these conformers is slightly above 0.6 at the start of the reaction, increases until it reaches a value of about 0.65 at 20 min, and then decreases to reach a constant value of about 0.3 at 150 min through 250 min.

The relative abundance for peak 3 from CE, which has an average electrophoretic mobility of $(5.4 \pm 0.3) \times 10^{-9}$ m^2/V s, starts at about 0.3; it then increases until it reaches a plateau slightly below 0.5 from 75 to 125 min. Thereafter, the relative abundance of peak 3 decreases until it reaches a value of about 0.1 between 225 and 250 min. This compares nicely to a combination of conformers C, D, and E from IMS; the sum of relative abundances of these conformers starts slightly above 0.1, then increases until reaching a plateau of slightly below 0.5 from 90 to 130 min, and subsequently decreases until reaching a value of about 0.1 at 225 min through 250 min.

Further confidence in the assignment for this conformer combination comes from analysis of the peak center, x_c, over the transition time (Table S1 and Figure S5). The standard deviation for the peak center for peak 3 is much larger than that of the other CE peaks. Noticeably, the peak center seems to have a consistent value of 5.15×10^{-9} m^2/V s at the start of the reaction and 5.85×10^{-9} m^2/V s at the end of the reaction. The shift is quite rapid and occurs around the transition time when D + E surpasses C in relative abundance in the IMS data (Figure S6). Although this would support the idea of peak 3 containing distinct conformers, attempts to resolve the two peaks mathematically by fitting with an additional peak were unsuccessful, as they did not lead to a convergent fit.

Peak 4 from the CE data, which has an average electrophoretic mobility of $(4.96 \pm 0.03) \times 10^{-9}$ m^2/V s, is unobservable at the beginning of the transition. It is first observed after about 70 min, and it then increases until reaching a plateau at a relative abundance value of about 0.65 from 210 to 250 min. This compares well to peak F from IMS, the PPII helix and major final product, which is unobservable at the start and is first detected at about 75 min; thereafter, it increases until also reaching a plateau at a value of about 0.6 from 175 min through 250 min.

Lastly, about 150 min into the transition, we can observe a small peak 5 in the CE data, with an average electrophoretic mobility of $(6.47 \pm 0.05) \times 10^{-9}$ m^2/V s. It maintains a consistently low relative abundance of about 0.01 until the end of the reaction, which is comparable to the behavior of peak H from the IMS data.

The most notable differences between the combined IMS and CE data sets are at the start of the reaction, and in our CE experiments, we found slight variance in the initial relative abundance of each component (Figures S7 and S8). This is most likely caused by the different drying methods used between the two methods, leading to differing amounts of propanol being retained in the structure between CE and IMS experiments and within replicates of the CE experiment. As the reaction proceeds toward equilibrium, the fit between the two experiments becomes much more pronounced; at the tail end of the reaction between 200 to 250 min, all 5 CE peaks and combinations of IMS data match very consistently. Key transition times observed in the IMS data are also reproduced in the CE data: the dominance of F (peak 4) over A (peak 1) at 75−80 min, the dominance of F over B + G (peak 2) at 140−145 min, and the dominance of F over C + D + E (peak 3) at 150−155 min, and the temporary dominance of C + D + E (peak 3) over B + G (peak 2) beginning at 65−85 min and ending at 150−155 min.

Structure and Charge Implications. As both CE and IMS separate ions as a function of charge and size, it is tempting to make direct comparisons of ion sizes. By comparing gas-phase collision cross sections from IMS to the results of molecular

DOI: 10.1021/acs.analchem.6b02424
Anal. Chem. 2016, 88, 10933−10939

dynamics simulations of desolvated structures, solution-phase structures have been proposed for each of the intermediates.[16] However, although these solution-phase structures are modeled in terms of cis−trans isomerism, they do not reflect actual solvation conditions or the movement of bonds beyond the peptide bond. The ion size in CE corresponds to the solvated species. In addition, our direct measurement in CE gives us a ratio of charge and size, and differences in either variable can contribute to differences in observed mobility.

We can, however, make semiquantitative comparisons for the two conformers that are more fully characterized and assumed to be more structurally constrained: the PPI (A in IMS and peak 1 in CE) and PPII (F in IMS and peak 4 in CE) helices. As both of these structures are rod-like, a theoretical hydrodynamic radius can be calculated using eq 4. However, we note that these structures may not be perfectly rod-like; it is possible that distortions in bonding angles lead to a different or more compact geometry. On the basis of the literature value of a helical rise per residue of 3.1 Å for the PPII helix,[57] this conformer of Pro13 would have an expected length of 40.3 Å. With a cylindrical diameter of approximately 8.4 Å, the theoretical R_h of the PPII helix is thus 10.2 Å. Although this value ignores entrained solvent, it compares well with our experimental findings; on the basis of our measured electrophoretic mobility and solution viscosity (1.68 ± 0.01 mPa s), the singly charged $[PPII + H]^+$ ion would have an R_h of 10.4 ± 0.1 Å.

In contrast, the PPI helix is described with a helical rise of only 1.9 Å.[57] With a cylindrical diameter of approximately 9.5 Å, the theoretical R_h of the PPI helix is 8.3 Å. We would thus expect PPI to have a higher electrophoretic mobility than PPII, as it is smaller. However, our experimental results show the opposite; PPI has a slower arrival time and lower electrophoretic mobility than PPII. The experimental hydrodynamic radius for $[PPI + H]^+$ is 10.9 ± 0.2 Å. The difference between the calculated and experimental hydrodynamic radius likely arises from an effective charge on PPI of less than +1,[58] which would be facilitated by the presence of 1-propanol and the more hydrophobic exterior of the PPI helix.[59,60] This and alternative explanations, including solvation effects, could be explored through rigorous simulation of the solvated system.

CONCLUSIONS

Ion mobility has provided a window into the process of peptide and protein folding.[16] One assumption that has been made in these ion mobility experiments is that gas-phase measurements reflect solution-phase populations. This work demonstrates that this is a reality for the polyproline system. Although capillary electrophoresis was not able to resolve all eight conformers involved in the transition of Pro13 from PPI to PPII, solution-phase intermediates were directly observed and their concentrations followed the same profiles as a function of time as seen in ion mobility. Detailed modeling of solution-phase structures is necessary to more fully characterize these intermediates and to confirm, or contradict, specific structures derived from gas-phase measurements.

ASSOCIATED CONTENT

Supporting Information

The Supporting Information is available free of charge on the ACS Publications website at DOI: 10.1021/acs.analchem.6b02424.

Full Haarhoff-Van der Linde function for CE peak fitting, Table S1, and Figures S1−S8 (PDF)

AUTHOR INFORMATION

Corresponding Author

*E-mail: hollidaya@moravian.edu.

Present Address

[‖]L.S.: Department of Chemistry, Washington University in St. Louis, St. Louis, MO 63130.

Notes

The authors declare no competing financial interest.

REFERENCES

(1) Hoaglund-Hyzer, C. S.; Counterman, A. E.; Clemmer, D. E. *Chem. Rev.* **1999**, *99*, 3037−3079.
(2) Bohrer, B. C.; Merenbloom, S. I.; Koeniger, S. L.; Hilderbrand, A. E.; Clemmer, D. E. *Annu. Rev. Anal. Chem.* **2008**, *1*, 293−327.
(3) Wyttenbach, T.; Pierson, N. A.; Clemmer, D. E.; Bowers, M. T. *Annu. Rev. Phys. Chem.* **2014**, *65*, 175−196.
(4) Lanucara, F.; Holman, S. W.; Gray, C. J.; Eyers, C. E. *Nat. Chem.* **2014**, *6*, 281−294.
(5) Loo, J. A.; Edmonds, C. G.; Smith, R. D. *Science* **1990**, *248*, 201−204.
(6) Suckau, D.; Shi, Y.; Beu, S. C.; Senko, M. W.; Quinn, J. P.; Wampler, F. M.; McLafferty, F. W. *Proc. Natl. Acad. Sci. U. S. A.* **1993**, *90*, 790−793.
(7) Pan, Y.; Brown, L.; Konermann, L. *Int. J. Mass Spectrom.* **2011**, *302*, 3−11.
(8) Breuker, K.; McLafferty, F. W. *Proc. Natl. Acad. Sci. U. S. A.* **2008**, *105*, 18145−18152.
(9) Pierson, N. A.; Chen, L.; Valentine, S. J.; Russell, D. H.; Clemmer, D. E. *J. Am. Chem. Soc.* **2011**, *133*, 13810−13813.
(10) Bush, M. F.; Hall, Z.; Giles, K.; Hoyes, J.; Robinson, C. V.; Ruotolo, B. T. *Anal. Chem.* **2010**, *82*, 9557−9565.
(11) Chen, L.; Gao, Y. Q.; Russell, D. H. *J. Phys. Chem. A* **2012**, *116*, 689−696.
(12) Bleiholder, C.; Do, T. D.; Wu, C.; Economou, N. J.; Bernstein, S. S.; Buratto, S. K.; Shea, J.-E.; Bowers, M. T. *J. Am. Chem. Soc.* **2013**, *135*, 16926−16937.
(13) Counterman, A. E.; Clemmer, D. E. *J. Phys. Chem. B* **2004**, *108*, 4885−4898.
(14) Mesleh, M. F.; Hunter, J. M.; Shvartsburg, A. A.; Schatz, G. C.; Jarrold, M. F. *J. Phys. Chem.* **1996**, *100*, 16082−16086.
(15) Silveira, J. A.; Fort, K. L.; Kim, D.; Servage, K. A.; Pierson, N. A.; Clemmer, D. E.; Russell, D. H. *J. Am. Chem. Soc.* **2013**, *135*, 19147−19153.
(16) Shi, L.; Holliday, A. E.; Shi, H.; Zhu, F.; Ewing, M. A.; Russell, D. H.; Clemmer, D. E. *J. Am. Chem. Soc.* **2014**, *136*, 12702−12711.
(17) Silveira, J. A.; Servage, K. A.; Gamage, C. M.; Russell, D. H. *J. Phys. Chem. A* **2013**, *117*, 953.
(18) Baumketner, A.; Bernstein, S. L.; Wyttenbach, T.; Bitan, G.; Teplow, D. B.; Bowers, M. T.; Shea, J.-E. *Protein Sci.* **2006**, *15*, 420−428.
(19) Ruotolo, B. T.; Robinson, C. V. *Curr. Opin. Chem. Biol.* **2006**, *10*, 402−408.
(20) Wyttenbach, T.; Bowers, M. T. *J. Phys. Chem. B* **2011**, *115*, 12266−12275.
(21) Hall, Z.; Politis, A.; Bush, M. F.; Smith, L. J.; Robinson, C. V. *J. Am. Chem. Soc.* **2012**, *134*, 3429−3438.
(22) Stellwagen, E.; Ledger, R. *Anal. Biochem.* **2003**, *321*, 167−173.
(23) Gavina, J. M. A.; Britz-McKibbin, P. *Curr. Anal. Chem.* **2007**, *3*, 17−31.
(24) Rochu, D.; Ducret, G.; Ribes, F.; Vanin, S.; Masson, P. *Electrophoresis* **1999**, *20*, 1586−1594.
(25) Hilser, V. J.; Freire, E. *Anal. Biochem.* **1995**, *224*, 465−485.
(26) Stutz, H.; Wallner, M.; Malissa, H.; Bordin, G.; Rodriguez, A. R. *Electrophoresis* **2005**, *26*, 1089−1105.

DOI: 10.1021/acs.analchem.6b02424
Anal. Chem. 2016, 88, 10933−10939

(27) Verzola, B.; Fogolari, F.; Righetti, P. G. *Electrophoresis* **2001**, *22*, 3728−3735.
(28) de Kort, B. J.; de Jong, G. J.; Somsen, G. W. *Analyst* **2013**, *138*, 4550−4557.
(29) de Kort, B. J.; ten Kate, G. A.; de Jong, G. J.; Somsen, G. W. *Anal. Chem.* **2011**, *83*, 6060−6067.
(30) Skelsey, K. R.; Bushey, M. M. *J. Chromatogr. Sci.* **1996**, *34*, 85−91.
(31) Clouthier, C. M.; Mironov, G. G.; Okhonin, V.; Berezovski, M. V.; Keillor, J. W. *Angew. Chem., Int. Ed.* **2012**, *51*, 12464.
(32) Jensen, P. K.; Lee, C. S.; King, J. A. *Anal. Chem.* **1998**, *70*, 730−736.
(33) Pal, D.; Chakrabarti, P. *J. Mol. Biol.* **1999**, *294*, 271−288.
(34) IUPAC-IUB Commission on Biochemical Nomenclature. *Biochemistry* **1970**, *9*, 3471−3479.
(35) Traub, W.; Shmueli, U. *Nature* **1963**, *198*, 1165.
(36) Swenson, C. A.; Formanek, R. *J. Phys. Chem.* **1967**, *71*, 4073−4077.
(37) Forsythe, K. H.; Hopfinger, A. J. *Macromolecules* **1973**, *6*, 423−437.
(38) Cheng, H. N.; Bovey, F. A. *Biopolymers* **1977**, *16*, 1465−1472.
(39) Chandrudu, S.; Simerska, P.; Toth, I. *Molecules* **2013**, *18*, 4373−4388.
(40) Koeniger, S. L.; Merenbloom, S. I.; Valentine, S. J.; Jarrold, M. F.; Udseth, H. R.; Smith, R. D.; Clemmer, D. E. *Anal. Chem.* **2006**, *78*, 4161−4174.
(41) Schaffer, S. A.; Tang, K. Q.; Anderson, G. A.; Prior, D. C.; Udseth, H. R.; Smith, R. D. *Rapid Commun. Mass Spectrom.* **1997**, *11*, 1813−1817.
(42) Hoaglund, C. S.; Valentine, S. J.; Sporleder, C. R.; Reilly, J. P.; Clemmer, D. E. *Anal. Chem.* **1998**, *70*, 2236−2242.
(43) Mason, E. A.; McDaniel, E. W. *Transport Properties of Ions in Gases*; Wiley: New York, 1988.
(44) Gas, B.; Stedry, M.; Kenndler, E. *Electrophoresis* **1997**, *18*, 2123−2133.
(45) Mikkers, F. E. P.; Everarts, F. M.; Verheggen, T. P. E. M. *J. Chromatogr.* **1979**, *169*, 1−10.
(46) Sustacek, V.; Foret, F.; Bocek, P. *J. Chromatogr.* **1991**, *545*, 239−248.
(47) Poppe, H. *Anal. Chem.* **1992**, *64*, 1908−1919.
(48) Dubský, P.; Dvořák, M.; Műllerová, L.; Gaš, B. *Electrophoresis* **2015**, *36*, 655−661.
(49) Erny, G.; Bergström, E.; Goodall, D. *Anal. Chem.* **2001**, *73*, 4862−4872.
(50) Erny, G.; Bergström, E.; Goodall, D. *J. Chromatogr. A* **2002**, *959*, 229−239.
(51) Schmitt-Kopplin, P.; Garmash, A.; Kudryavtsev, A. V.; Menzinger, F.; Perminova, I.; Hertkorn, N.; Freitag, D.; Petrosyan, V.; Kettrup, A. *Electrophoresis* **2001**, *22*, 77−87.
(52) Jorgenson, J. J.; Lukacs, K. D. *Anal. Chem.* **1981**, *53*, 1298−1302.
(53) Grossman, P. D. In *Capillary Electrophoresis: Theory and Practice*; Grossman, P. D., Colburn, J. C., Eds.; Academic Press, Inc.: San Diego, CA, 1992; pp 111−132.
(54) Johnson, J. F.; Martin, J. R.; Porter, R. S. Determination of Viscosity. In *Physical Methods of Chemistry, Part VI*; Weissberger, A. L., Rossiter, B. W., Eds.; Wiley-Interscience: New York, 1977; p 63.
(55) Ortega, A.; García de la Torre, J. *J. Chem. Phys.* **2003**, *119*, 9914−9919.
(56) Cortajarena, A. L.; Lois, G.; Sherman, E.; O'Hern, C. S.; Regan, L.; Haran, G. *J. Mol. Biol.* **2008**, *382*, 203−212.
(57) Köhler, S. D.; Weber, A.; Howard, S. P.; Welte, W.; Drescher, M. *Protein Sci.* **2010**, *19*, 625−630.
(58) Skoog, B.; Wichman, A. *TrAC, Trends Anal. Chem.* **1986**, *5*, 82−83.
(59) Grossman, P. D.; Wilson, K. J.; Petrie, G.; Lauer, H. H. *Anal. Biochem.* **1988**, *173*, 265−270.
(60) Walhagen, K.; Huber, M. I.; Hennessy, T. P.; Hearn, M. T. W. *Biopolymers* **2003**, *71*, 429−453.

DOI: 10.1021/acs.analchem.6b02424
Anal. Chem. 2016, 88, 10933−10939